

KNN-MMD: Cross Domain Wireless Sensing via Local Distribution Alignment

Zijian Zhao, Zhijie Cai, Tingwei Chen, Xiaoyang Li, Hang Li, Qimei Chen, Guangxu Zhu

Abstract—Wireless sensing has recently found widespread applications in diverse environments, including homes, offices, and public spaces. By analyzing patterns in channel state information (CSI), it is possible to infer human actions for tasks such as person identification, gesture recognition, and fall detection. However, CSI is highly sensitive to environmental changes, where even minor alterations can significantly distort the CSI patterns. This sensitivity often leads to performance degradation or outright failure when applying wireless sensing models trained in one environment to another. To address this challenge, Domain Alignment (DAL) has been widely adopted for cross-domain classification tasks, as it focuses on aligning the global distributions of the source and target domains in feature space. Despite its popularity, DAL often neglects inter-category relationships, which can lead to misalignment between categories across domains, even when global alignment is achieved. To overcome these limitations, we propose K-Nearest Neighbors Maximum Mean Discrepancy (KNN-MMD), a novel few-shot method for cross-domain wireless sensing. Our approach begins by constructing a “help set” using K-Nearest Neighbors (KNN) from the target domain, enabling local alignment between the source and target domains within each category using Maximum Mean Discrepancy (MMD). Additionally, we address a key instability issue commonly observed in cross-domain methods, where model performance fluctuates sharply between epochs. Further, most existing methods struggle to determine an optimal stopping point during training due to the absence of labeled data from the target domain. Our method resolves this by excluding the support set from the target domain during training and employing it as a validation set to determine the stopping criterion. We evaluate the effectiveness of the proposed method across several cross-domain Wi-Fi sensing tasks, including gesture recognition, person identification, fall detection, and action recognition, using both a public dataset and a self-collected dataset. In a one-shot scenario, our method achieves accuracy rates of 93.26%, 81.84%, 77.62%, and 75.30% for the respective tasks. To support future research, we will release our code and dataset to the public upon publication.

Index Terms—Few-shot Learning, K-Nearest Neighbors, Maximum Mean Discrepancy, Cross-domain Wi-Fi Sensing, Channel Statement Information

I. INTRODUCTION

These days, the importance of wireless sensing has grown significantly, driven by advancements in technology and the increasing demand for efficient monitoring solutions. Wireless sensing has found applications in various fields such as fall detection [1], person localization [2], and people identification [3]. Among the various manners, Wi-Fi sensing stands out as a popular method with numerous advantages, as outlined in Table I. First, Wi-Fi sensing is contactless as the object to be detected does not need to carry a device like a smartphone or smartwatch. Second, Wi-Fi sensing is privacy-preserving compared with camera. Third, Wi-Fi sensing is insensitive to occlusions and illumination conditions since its electromagnetic wave operates on a frequency band that can penetrate walls. Moreover, Wi-Fi sensing is ubiquitous, with over 19.5 billion Wi-Fi devices deployed globally [4]. With an appropriate algorithm that enables its sensing function, ubiquitous sensing function can be realized in various environments, such as homes, offices, and public spaces. Last but not least, Wi-Fi sensing has lower cost compared to dedicated radars.

Given the released tool that works with some specific types of commercial Network Interface Cards (NIC) [5], the Channel State Information (CSI) can be obtained, which describes how the wireless signals fade during the propagation from the sender to the receiver. By using this CSI data collection tool, a series of research employing commercial Wi-Fi NICs for different kinds of tasks. Moreover, a dedicated IEEE standard for Wi-Fi sensing named IEEE 802.11bf is approved [6] to enable faster development and practicalization of Wi-Fi sensing technologies. However, since the Orthogonal Frequency Division Multiplexing (OFDM) waveforms employed by Wi-Fi are designed for communication purpose without sensing optimization, it is thus challenging to apply physical models to infer and sense the ambient environment from the CSI measurements.

As a result, most Wi-Fi sensing methods rely on data-driven approach via machine learning [7], [8], especially for fine-grained tasks like gesture recognition [9]. However, even minor environmental changes can drastically alter the CSI patterns and significantly degrade the performance of the trained model. This environmental variability leads to a domain shift - a discrepancy between the training data distribution and real-world deployment conditions. Given the strong dependence of the training data, such domain shifts can severely undermine the generalization capability. This scenario is known as a cross-domain problem in machine learning, where the source domain (training data) and target domain

* Corresponding Author: Guangxu Zhu

Zijian Zhao is with Shenzhen Research Institute of Big Data, Shenzhen 518115, China, and also with the School of Computer Science and Engineering, Sun Yat-sen University, Guangzhou 510275, China (e-mail: zhaozj28@mail2.sysu.edu.cn)

Zhijie Cai, Tingwei Chen, Xiaoyang Li, Hang Li, and Guangxu Zhu are with the Shenzhen Research Institute of Big Data, The Chinese University of Hong Kong (Shenzhen), Shenzhen 518115, China (e-mail: zhijecai@link.cuhk.edu.cn; tingweichen@link.cuhk.edu.cn; lixiayoung@sribd.cn; hangdavidli@sribd.cn; gxzhu@sribd.cn)

Qimei Chen is with the School of Electronic Information, Wuhan University, Wuhan, 430072, China (e-mail: chenqimei@whu.edu.cn).

TABLE I
COMPARISON OF COMMON SENSING METHODS

	Coverage	Privacy	Cost
Camera	Low (affected by occlusion/lighting)	Low	Moderate
Millimeter Wave	Moderate	Moderate	High
Infrared Sensor	Moderate	High	Moderate
Wi-Fi	High (non-line-of-sight, all-day)	High	Low

(testing data) have different underlying distributions or feature spaces.

In fields like Computer Vision (CV) and Natural Language Processing (NLP), where large datasets are available in these common modalities, it is relatively easy to solve such cross-domain problems by training large models with vast amount of data [10]. However, in Wi-Fi sensing, the limited public datasets often have different formats, making it challenging to use them together to train a model. Additionally, collecting large CSI datasets on one's own is not easy. Therefore, it is needed to develop a powerful yet adaptable small model that can quickly adapt to new environments, which has emerged as an important research direction in Wi-Fi sensing.

As the most common method for cross-domain tasks, Domain Adaptation (DA) has been widely utilized in cross-domain Wi-Fi sensing. DA focuses on leveraging knowledge from a source domain to enhance model performance on a related but different target domain. Among these methods, Domain Alignment (DAL), which aims to map the source and target domains to the same distribution, is one of the most popular approaches and has been extensively applied in Wi-Fi sensing [11]–[17]. However, as shown in Fig. 1, the global alignment of traditional DAL methods can lead to incorrect alignments within categories, which can hinder the effectiveness of the classification boundary trained in the source domain when applied to the target domain. Another widely recognized issue in DA is low stability: the model's performance on the testing set can be unstable during training (as referenced in [18] and Section IV-D), with accuracy varying sharply between successive epochs. This instability suggests that simply stopping the model training at a fixed epoch may result in poor performance. If we wish to implement an early stopping method, we require labeled validation data from the target domain. However, the only labeled data available from the target domain is the support set, which is often a subset of the training set and cannot be used as a validation set.

To address the limitations of traditional DAL methods in cross-domain Wi-Fi sensing, we propose a novel Few-Shot Learning (FSL) framework, called K-Nearest Neighbors Maximum Mean Discrepancy (KNN-MMD). Our approach introduces a local distribution alignment strategy that aligns the source and target domains within each category, rather than globally aligning their overall data distributions. This refinement enhances the effectiveness of traditional DAL techniques by addressing inter-category misalignments. Additionally, our framework ensures that the support set is excluded from the network's training process, enabling the implementation of an early stopping strategy based on support set performance. This

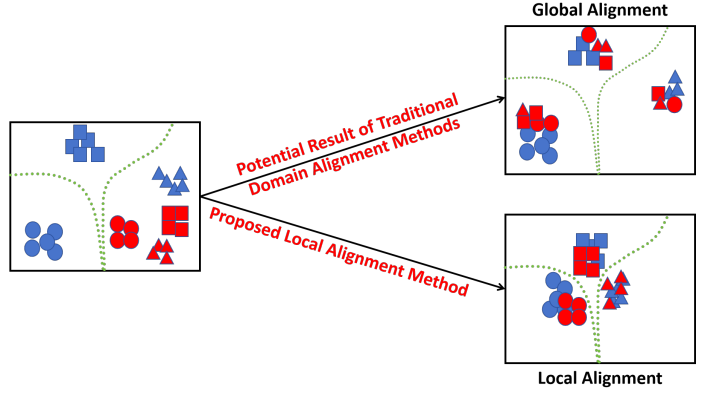


Fig. 1. Distinguishing Local Alignment from Global Alignment: Different colors represent different domains, different shapes represent different categories, and the green line represents the classification boundary, which remains consistent across subsequent figures.

ensures stable and consistent target domain performance while avoiding the challenges faced by traditional DAL methods in determining an optimal stopping point.

The key contributions of this work are summarized as follows:

1. A Few-Shot Learning Framework with Local Alignment: We present KNN-MMD, a novel FSL framework tailored for cross-domain Wi-Fi sensing. Unlike traditional DAL methods that rely on global alignment, our framework leverages a category-specific alignment strategy to improve accuracy and robustness. Specifically, we use K-Nearest Neighbors (KNN) to assign pseudo-labels to the target domain and construct a high-confidence “help set.” This help set, in combination with the source domain training data, is then used to perform local alignment during the training of the classification network.

2. An Early Stopping Strategy Using the Support Set: Our framework introduces a practical early stopping mechanism by excluding the support set from the training process while using it as a validation set for monitoring accuracy and loss. This approach ensures the training process concludes at an optimal point, maintaining strong performance in the target domain. Traditional DAL methods often lack such a mechanism, leading to unstable or suboptimal performance.

3. Comprehensive Experimental Validation: We extensively evaluate our method across multiple Wi-Fi sensing tasks, including gesture recognition, person identification, fall detection, and action recognition. Experimental results demonstrate that our framework outperforms existing models in both accuracy and stability, showcasing its effectiveness in real-world cross-domain Wi-Fi sensing scenarios.

The structure of this paper is as follows. In Section II, we first analyze the cross-domain Wi-Fi sensing tasks and illustrate the limitations of traditional DA methods. In Section III, we revisit the cross-domain task and propose our local alignment method in detail. In Section IV, we use a series of experiments to demonstrate the efficiency and stability of our method. Finally, in Section V, we conclude the paper and provide some points for future research.

II. PROBLEM STATEMENT AND EXISTING METHODS

A. Wi-Fi Sensing Principle

In Wi-Fi sensing, CSI is one of the most commonly used features. The channel between the transmitter and receiver can be influenced when encountering dynamic or static objects. The RX will then receive the multipath superimposed signals from refraction, reflection, and scattering. By analyzing the received CSI, we can obtain information about the environment and behavior. The channel model can be mathematically represented as:

$$Y = HX + N, \quad (1)$$

where Y and X are the matrices of the received and transmitted signals, respectively, N is the noise, and H is the estimate of the Channel Frequency Response (CFR) of the wireless channel, which contains information about the amplitudes, phases, and delays of the multipath components. It can also be represented as:

$$H = ||H||e^{j\angle H} \quad (2)$$

where $||H||$ and $\angle H$ denote the amplitude and phase of the CSI measurement, respectively.

For most Wi-Fi sensing tasks, when an object moves, the CSI changes according to patterns specific to the movement. By analyzing these changes in CSI values, the object motions can be detected. Compared to other Wi-Fi signals, such as the Received Signal Strength Indicator (RSSI), CSI captures fine-grained features, thus providing more precise information for Wi-Fi sensing.

B. Domain Shift Issue in Wi-Fi Sensing

To facilitate understanding, we first define the symbols and the cross-domain scenarios. In the following, the variables x and y refer to the input data and output label, respectively. θ represents the network parameters. P_s and P_t represent the classification probabilities of each category in the source domain and target domain, respectively. Furthermore, the focus of this paper is primarily on the few-shot cross-domain task. Most available data is in the source domain expect n labeled samples for each category in the target domain. This scenario is often referred to as the n-shot problem. In addition, we also have some unlabeled data from the target domain. Our objective is to accurately classify these unlabeled data. For the sake of simplicity, we will refer to the labeled data from the source domain as the training set, and the labeled data from the target domain as the support set.

In cross-domain Wi-Fi sensing, the most significant challenge is the substantial variation in data distribution across different domains, which causes models trained in the source

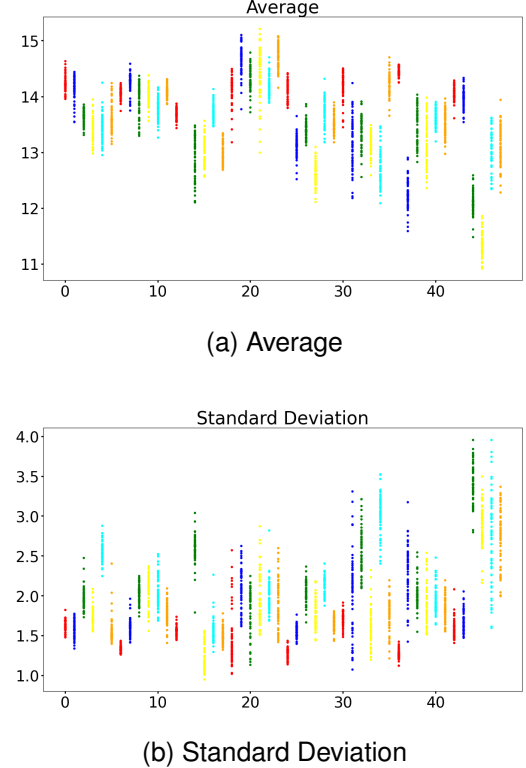


Fig. 2. Average and Standard Deviation of CSI Amplitude (WiGesture Dataset) [3]: Each point represents a 1s sample. The x-axis represents different people and action IDs, while different colors represent different actions.

domain to often fail in the target domain. For better illustration, we use WiGesture dataset [3], which contains the CSI collected from 8 individuals performing 6 different gesture actions, to illustrate the domain shift problem in detail. For the gesture recognition or action classification task, we take different people as different domains. And for the people identification task, we take different actions as different domains. Fig. 2 depicts the distribution of mean and standard deviation of CSI amplitude across various individuals and actions. It is evident that even for the same action, individuals exhibit distinct data distributions. Likewise, Fig. 3a and 3b display the Uniform Manifold Approximation and Projection (UMAP) based data reduction [19] results (we will introduce this data dimension reduction method in Section III-D1). It is apparent that within a single individual, different actions exhibit significant dissimilarities. However, when considering different individuals, the boundaries separating different actions become less distinct. These findings imply that it is challenging to generalize the learned features from one set of individuals to others. In Fig. 3c, a Resnet18 [20] is trained by setting the people with IDs 1-7 as the source domain and people with ID 0 as the target domain. It can be observed that the trained Resnet18 can distinguish different actions in the source domain but fail to distinguish different actions in the target domain. This is mainly because even for the same action, different people have distinct behavioral patterns, which can lead to significant gaps in the CSI patterns between individuals. As a result, to make the model perform well in

TABLE II
COMPARISON OF DIFFERENT DA METHODS

Representative Methods	Metric-based Method	Learning-based Method	Domain Alignment Method	Ours
Sensitivity to Quality of Support Set	KNN [21], K-means [22]	Siamese [23], Triplet Network [24]	MMD [25], GFK [26], [27]	KNN-MMD
Stability	High	Moderate	None	Low
Assumption $P_t(y x) = P_s(y x)$	No	Some methods require it [28]	Yes	High

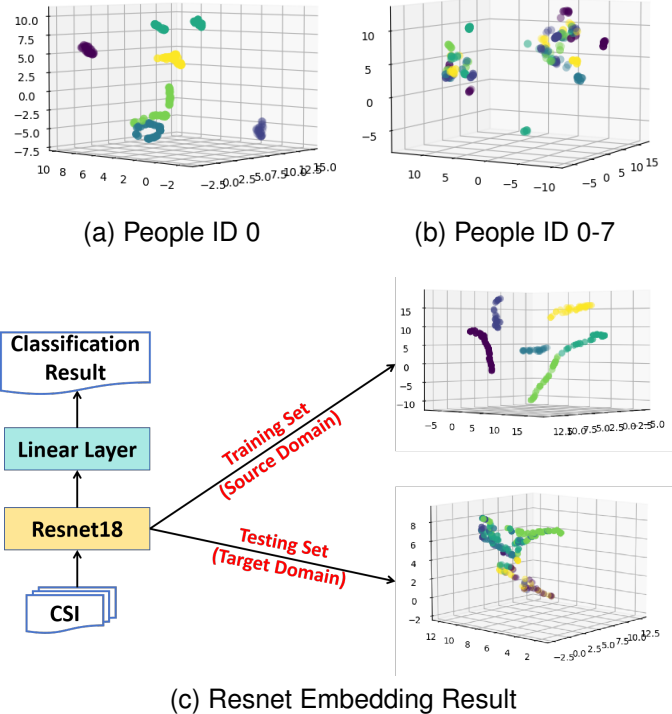


Fig. 3. Data Dimension Reduction Results of the WiGesture Dataset [3]: Different colors represent different categories. The data dimensions have been reduced to three for visualization, corresponding to the three axes in the figures. They remain consistent across subsequent figures.

the target domain, it is necessary to address the domain shift (cross-domain) problem.

C. Existing Domain Adaptation Methods

As the most prevalent method in cross-domain tasks, DA encompasses various classification approaches. We primarily follow [29], [30], categorizing DA into three types: metric-based methods, learning-based methods, and DAL methods. In practice, a method may belong to multiple categories, however, this paper focuses on their primary classifications: metric-based methods refer mainly to traditional machine learning approaches that do not involve training, learning-based methods pertain to those associated with novel network architectures, and DAL methods primarily address the alignment of feature spaces between source and target domains.

The core idea of metric-based methods is to learn a good sample representation and metric. However, most metric-based methods only depend on the support set without using the training set in source domain sufficiently. As a result, these methods are heavily influenced by the quality of the support

set, which can lead to unstable performance and the waste of the training set.

With the development of deep learning, there have been many learning-based methods for cross-domain tasks in recent years, including transfer learning [31], meta learning [32], FSL [33]. However, an important practical problem of these methods is that we do not know when to stop the model training. Since there is often a significant gap between the source and target domains, we cannot reliably infer the model's performance on the target domain based on its performance on the source domain. As a result, the typical early stop strategies cannot be easily applied in such scenarios.

DAL methods aim to map the source domain and target domain to a common feature distribution, where the data in the two domains can have the same distribution in the new space. However, most DAL methods, such as MMD [25], Kernel Mean Matching (KMM) [34], and Subspace Geodesic Flow (SGF) [35], rely on the assumption that the conditional probabilities in the source domain and target domain are the same, i.e., $P_t(y|x) = P_s(y|x) = P(y|x)$. To estimate $P(y|x)$, the network parameters θ need to be learned to achieve $P(y|x; \theta) = P(y|x)$. However, due to $P_t(x) \neq P_s(x)$, the $P(y|x; \theta)$ learned from the source domain cannot generalize to the target domain. Consequently, these traditional methods can be seen as finding a latent space where the input data from the source domain and target domain are mapped to the same distribution, i.e., $P_t(x) = P_s(x)$. This allows the model to learn the parameter θ more effectively and accurately. However, in many practical scenarios, the assumption $P_t(y|x) = P_s(y|x)$ is not met. This has been demonstrated in our experiments (Section IV-C) as well as our previous research [18], where traditional DAL methods even failed in cross-domain Wi-Fi sensing tasks.

In conclusion, the quality of the support set makes the performance of metric-based methods unstable. For learning-based methods, they also use source domain data to train, and the influence of the support set is not as significant as for metric-based methods. However, it's hard to identify when to stop the training process, and the accuracy in the test set always has significant fluctuations during training (shown in Section IV-C). Finally, most DAL methods do not require a support set for training, and they are not affected by the quality of the support set. But they mainly rely on the assumption of $P_t(y|x) = P_s(y|x)$, which is not always established in practice. Thus, the model would easily fail.

In addition, some other researches have also identified the limitations of traditional DAL methods. Tian et al. [36] utilize KNN [21] to identify the nearest samples in the entire data domain to each sample in the source domain, expanding the distance between neighboring samples from different

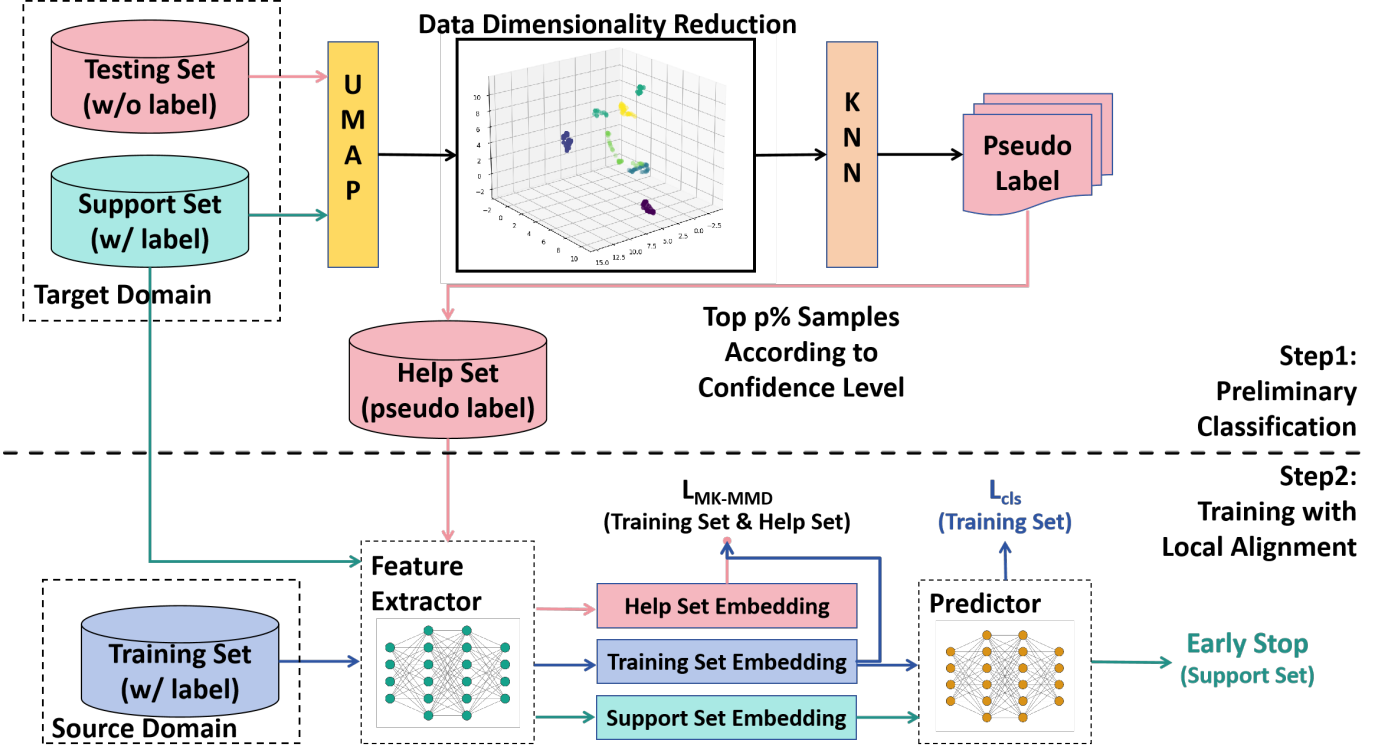


Fig. 4. Workflow: Our method primarily consists of two steps. In Step 1, we use KNN to preliminarily classify the testing set and select the top $p\%$ of samples with the highest classification confidence levels to construct a help set. In Step 2, we train a network for the final classification, using local alignment based on the training set and the help set. Simultaneously, we employ an early stop strategy according to the classification accuracy in the support set.

categories in the source domain, and shrinking the distance between neighboring samples from the target domain under the assumption that such sample pairs share the same category. However, this approach may also lead to potential failures, as shown in Fig. 1. Though the source domain samples have a relatively small distance to their neighboring samples in the target domain and a large distance to other category samples in the source domain, it cannot guarantee accurate classification in the target domain. Li et al. [37] first generate pseudo-labels for samples in the target domain using a classifier trained in the source domain and then attempt to expand the distance between samples with different categories and shrink the distance between samples with the same category. However, due to the inherent gap between the source and target domains, the pseudo-labels generated in the first step may be inaccurate, which can adversely impact the subsequent steps.

III. METHODOLOGY

A. Overview

As discussed in previous section, traditional DAL methods cannot guarantee model performance. To solve this problem, we propose a local distribution alignment approach that aligns the distribution between the source domain and the target domain within each category. (The detailed mathematical analysis will be discussed in Section III-B.) However, the category labels in the testing set cannot be accessed during training, and it is also challenging to estimate the target domain distribution solely based on the limited labeled data in the support set. As a result, we propose a preliminary strategy

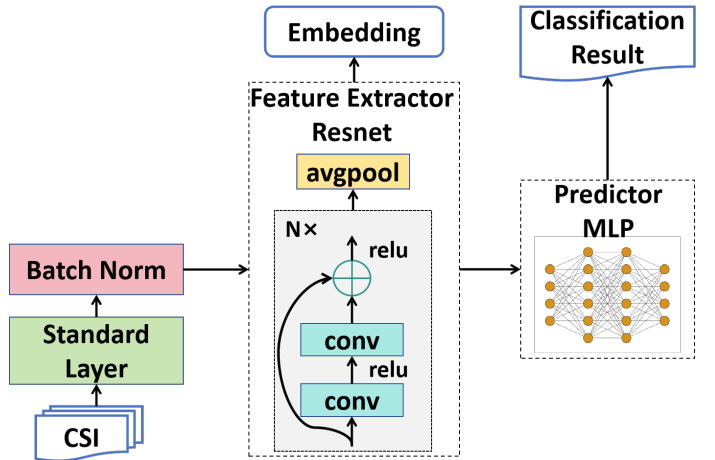


Fig. 5. Model Structure: We use the Resnet18 [20] as the feature extractor and a three-layer MLP as the predictor.

to first obtain some labels in the testing set to estimate the distribution.

As shown in Fig. 4, our method mainly has two steps: (1) Preliminary Classification and (2) Training Network with Local Alignment. In Step 1, we use KNN to preliminarily classify the testing set according to the support set. We then choose the samples with the highest classification confidence levels to construct a help set for Step 2. The help set will be used for the local alignment with the training set. In Step 2, we train a classification network with the MK-MMD loss function

to align the source domain and the target domain within each category. Additionally, we use an early stop strategy according to the classification accuracy in the support set, as it does not participate in the training and has the same distribution as the testing set. By this way, our training process can stop at a point where the testing set has a relatively high classification accuracy.

Before introducing our method in detail, let us describe the data format in our study. Each sample consists of two dimensions representing the data length l and subcarrier s , respectively. As we choose Resnet as the feature extractor, it requires an extra channel. Consequently, each sample has three dimensions, denoted as $x \in \mathbb{R}^{1 \times l \times s}$. The training set, support set, help set, and testing set are represented as X^{train} , $X^{support}$, X^{help} , and X^{test} , respectively, where the help set is not provided but generated by us.

B. Local Distribution Alignment

Let's reconsider the cross-domain classification task. As proposed in [38], the assumption $P_t(y|x) = P_s(y|x)$ is not met in most practical scenarios. As a result, we consider the case when $P_t(y|x) \neq P_s(y|x)$ and aim to find a feature space where, after mapping, $P_t(y|x') = P_s(y|x')$. In this feature space, we can train a classifier network to realize the final classification.

We can use the conditional probability formula to structure the relationship between $P_s(y|x)$ and $P_t(y|x)$ as:

$$\begin{aligned} P_s(y|x) &= P_t(y|x) \frac{P_s(x|y)P_s(y)}{P_s(x)} \frac{P_t(x)}{P_t(x|y)P_t(y)} \\ &= P_t(y|x) \frac{P_t(x)}{P_s(x)} \frac{P_s(x|y)}{P_t(x|y)} \frac{P_s(y)}{P_t(y)} \\ &= P_t(y|x) \frac{\sum_{y'} P_t(y')P_t(x|y')} {\sum_{y'} P_s(y')P_s(x|y')} \frac{P_s(x|y)}{P_t(x|y)} \frac{P_s(y)}{P_t(y)}, \end{aligned} \quad (3)$$

where y' represents the index of the category in the mapped feature space. In most cases, we have $P_s(y) \approx P_t(y)$, indicating that the label distribution is similar between the source and target domains. If we also have $P_t(x|y) \approx P_s(x|y)$, then $P_s(y|x) \approx P_t(y|x)$.

To realize distribution alignment, in this paper, we utilize the MK-MMD method, which is based on MMD. MMD measures the distance between two distributions and aims to map the source and target domains to a middle space with similar distributions.

If two distributions have exactly the same k -th central factorial moment for any k , then they are regarded following the same distribution. Since the k -th central factorial moment can be represented by the 1-st central factorial moment, i.e. the mean value, in a feature space, we can search for a mapping feature that maximizes the difference in means between the source and target domains. By minimizing the maximum distance, we can minimize the distribution difference between the two domains. Accordingly, MMD is defined as:

$$\text{MMD}[F, p, q] := \sup_{f \in F} |\mathbb{E}_p[f(x)] - \mathbb{E}_q[f(x)]|, \quad (4)$$

where F is the set of mapping functions in the Reproducing Kernel Hilbert Space (RKHS), p and q represent two

distributions, and \mathbb{E} denotes the expectation value. However, directly computing the mapping function can be challenging in practice. Therefore, kernel functions are often used to compute MMD as:

$$\begin{aligned} \text{MMD}[F, p, q] &= \sup_{f \in F} \left[\left| \frac{1}{n} \sum_{i=1}^n f(x_i^{(p)}) - \frac{1}{m} \sum_{i=1}^m f(x_i^{(q)}) \right|^2 \right]^{\frac{1}{2}} \\ &= \sup_{f \in F} \left[\frac{1}{n^2} \sum_{i=1}^n \sum_{j=1}^n f(x_i^{(p)}) f(x_j^{(p)}) \right. \\ &\quad \left. - \frac{2}{nm} \sum_{i=1}^n \sum_{j=1}^m f(x_i^{(p)}) f(x_j^{(q)}) + \frac{1}{m^2} \sum_{i=1}^m \sum_{j=1}^m f(x_i^{(q)}) f(x_j^{(q)}) \right]^{\frac{1}{2}} \\ &= \sup_k \left[\frac{1}{n^2} \sum_{i=1}^n \sum_{j=1}^n k(x_i^{(p)}, x_j^{(p)}) \right. \\ &\quad \left. - \frac{2}{nm} \sum_{i=1}^n \sum_{j=1}^m k(x_i^{(p)}, x_j^{(q)}) + \frac{1}{m^2} \sum_{i=1}^m \sum_{j=1}^m k(x_i^{(q)}, x_j^{(q)}) \right]^{\frac{1}{2}}, \end{aligned} \quad (5)$$

where $x_i^{(p)}$ represents the i -th sample from distribution p , n and m represent the sample sizes of distributions p and q respectively, and k denotes the kernel function of the mapping function f .

However, it is often difficult to find a kernel function that can realize the upper bound in practice. Therefore, Gretton et al. [39] proposed MK-MMD, which uses multiple kernel functions to approximate the upper bound, as:

$$\begin{aligned} \text{MK-MMD}^2[K, p, q] &= \sum_{h=1}^H \beta_h \left[\frac{1}{n^2} \sum_{i=1}^n \sum_{j=1}^n K_h(x_i^{(p)}, x_j^{(p)}) \right. \\ &\quad \left. - \frac{2}{nm} \sum_{i=1}^n \sum_{j=1}^m K_h(x_i^{(p)}, x_j^{(q)}) + \frac{1}{m^2} \sum_{i=1}^m \sum_{j=1}^m K_h(x_i^{(q)}, x_j^{(q)}) \right], \end{aligned} \quad (6)$$

where K is the set of kernel functions provided by the user, and β is a set of weights that satisfy $\sum_{h=1}^H \beta_h = 1$. During training, the MK-MMD loss function can be used in the embedding result of the source and target domains to encourage the feature extractor to map the source and target domain data to the same distribution in the intermediate feature space.

C. Model Structure

Our model architecture is illustrated in Fig. 6, which primarily consists of three components: a normalization layer, a feature extractor, and a final classifier. The normalization layer incorporates time-level standardization and batch normalization, helping to reduce the domain gap between different samples and facilitating the training process. Then we select the pre-trained ResNet18 [20] as the feature extractor because the Wi-Fi signal spectrum exhibits high similarity to images. Convolutional networks, which effectively extract local features, have demonstrated excellent performance in CSI classification [1], [18], [40]. Furthermore, inspired by transfer learning, the pre-trained parameters from image data provide a strong starting point for Wi-Fi sensing [41]. Finally, we employ a MLP to process the embeddings for classification. The detailed description is as follows:

First, we use a standard layer [3] as shown in Eq. 7:

$$\text{Std}(X_i^{(j)}) = \frac{X_i^{(j)} - E_{time}[X^{(j)}]}{\sqrt{D_{time}[X^{(j)}]}}, \quad (7)$$

where $X_i^{(j)}$ represents the i -th sample in the j -th subcarrier of the CSI sequence X , E and D denote the expectation and variance, respectively. The standardization operation is applied in the time dimension. In [3], it's noted that the distribution of CSI would have a significant difference in different time ranges, which could make the network difficult to converge. By standardization, the data distribution in the time dimension can be unified to a similar distribution, which helps to solve this problem, to a certain extent.

Then, the data is input to a batch normalization layer that normalizes each element along the batch dimension, as shown in Eq. 8:

$$\text{BN}(X) = \gamma \frac{X - E_{batch}[X]}{\sqrt{D_{batch}[X]}} + \beta, \quad (8)$$

where γ and β are learnable parameters. Batch normalization is a traditional method to deal with the covariate shift problem [42], which is similar to domain shift but with a smaller domain gap. As a result, we use it to deal with the domain shift problem.

Subsequently, the processed data is fed into Resnet to obtain the embedding, which serves as the feature space mapping mentioned in Section III-B. Finally, the MLP acts as a classifier, taking the embedding as input and producing the corresponding label as output. The network can be expressed as Eq. 9.

$$\begin{aligned} E &= \text{Resnet}(\text{BN}(\text{Std}(X))), \\ \hat{Y} &= \text{MLP}(E), \end{aligned} \quad (9)$$

where E is the embedding result, and \hat{Y} is the output.

D. Training Process

The training process consists of two main phases: preliminary classification and network training with local alignment. In order to align the source and target domains locally within each category, we need to know the labels of the target domain samples. However, since we have only a very limited labeled support set in the target domain, it is challenging to use these samples for alignment, as this typically requires a larger number of samples to capture statistical features effectively. To address this issue, we propose using KNN for preliminary classification of the target domain. Although KNN may not be very stable and often produces numerous incorrect classifications, we find that classification accuracy is closely related to the confidence level. By leveraging this insight, we can construct a helper set consisting of samples with high confidence levels, the majority of which are correctly classified in practice. During the network training phase, we use this helper set to achieve local alignment with the source domain training set. Finally, the trained network can be employed for final classification, demonstrating excellent performance on samples with low classification confidence from KNN. Moreover, since the support set does not participate in network

training, we can utilize it as a validation set to determine when to stop model training. In the following, we provide a detailed description of the two phases:

1) *Preliminary Classification*: Before applying KNN for preliminary classification, we need to flatten each sample to one-dimensional data, denoted as $x' \in R^{ls}$. Subsequently, we construct the target domain data $X'^{\text{target}} = [X'^{\text{support}}, X'^{\text{test}}]$. However, the data dimension ls is often too high, exceeding a thousand, which may lead to a high computational burden for KNN. Therefore, prior to using KNN, we aim to reduce the data dimension in X'^{target} via UMAP [19].

UMAP primarily involves four steps: constructing the nearest neighbor graph, approximating a fuzzy-simplicial set, optimizing the low-dimensional embedding using stochastic gradient descent, and finalizing the embedding after convergence. Since UMAP is not the primary focus of our research, we directly utilize the function implemented by the UMAP package in Python. For more details, interested readers can refer to the UMAP paper [19].

After performing dimension reduction, we utilize the KNN algorithm to classify the testing set based on the support set. For more detailed information on the KNN algorithm, please refer to the paper [21]. Briefly, for each sample in the testing set, we identify the nearest k samples from the support set using Gaussian distance as the distance measure. Subsequently, we determine the most frequent label among the identified neighbors as the classification result. In the case of a tie, we select the label of the nearest neighbor as the classification result.

Next, we select the top $p\%$ samples from the testing set to construct the help set based on the confidence level of classification. In our approach, the confidence is measured by calculating the distance between each sample in the testing set and its nearest neighbor in the support set with the same label. A smaller distance indicates higher confidence. Through experimentation, we have found this method to be effective. For instance, in the four tasks conducted in our experiment, when setting $p\%$ to 50%, the classification accuracy of the selected top $p\%$ samples consistently exceeds 90%, regardless of the values of k (the number of neighbors in KNN) and n (the number of samples per category in the support set for n-shot tasks). Hence, we consider these samples as the help set for the subsequent steps.

2) *Training Network with Local Alignment*: In Step 2, we train our network using the loss function consisting of three components, as presented in Eq. 10:

$$L = L_{cls} + L_{MMD}^{\text{local}} + L_{MMD}^{\text{global}}, \quad (10)$$

Firstly, L_{cls} represents the traditional cross-entropy loss function, which utilizes data solely from the training set. It is used to train the model to learn the basic classification capacity. Secondly, L_{MMD}^{local} represents the local MMD, which calculates the MK-MMD between the help set and the training set within

each category, as shown in Eq. (11):

$$L_{MMD}^{local} = \frac{1}{M} \sum_{i=1}^M \text{MK-MMD}(K, E^{train}, E^{help} | Y = i), \quad (11)$$

where E is the embedding result of Resnet, K is the given kernal list, and Y is the sample label. It's used to realize our local alignment. Additionally, we add an extra global MMD, which computes the MK-MMD between the entire help set and training set, following the conventional MMD approach, as represented in Eq. (12):

$$L_{MMD}^{global} = \text{MK-MMD}(K, E^{train}, E^{help}), \quad (12)$$

As mentioned previously, our primary focus lies on the local MMD rather than the global MMD. However, we include the global MMD to address potential challenges arising from an imbalanced distribution of samples among different labels within the help set. By incorporating the global MMD, we can mitigate this issue to some extent. For example, if we ensure $P_s(x|y) = P_t(x|y)$ for all y except $y = i$, and also make $P_t(x) = P_s(x)$, we can achieve $P_s(x|y = i) = P_t(x|y = i)$. Nonetheless, it is important to note that this approach has limitations when there is a significant lack of certain categories. Alternatively, we can employ other methods to generate the help set and address category imbalance. For example, within the testing set, we can directly select the top $p\%$ samples within each category or choose a fixed number of samples with the highest confidence level within each category. However, this may impact the accuracy of the help set to some extent.

Furthermore, as previously mentioned, many traditional FSL methods encounter the issue of determining when to stop training. Since their support sets are often involved in the training process, they are unable to obtain a valid set comparable to traditional machine learning methods for early stop. However, in our approach, since the support set is not included in the computation of the loss function, we can implement an early stop strategy based on the accuracy of the support set.

The early stop strategy is outlined in Algorithm 1. During the training, we keep track of the highest accuracy and the lowest value of the loss function in the support set. Each time the accuracy or the loss value is improved, we save the corresponding model parameters. When the epoch reaches the minimum training epoch e^{min} , if the validation accuracy does not improve and the validation loss does not decrease for consecutive $e^{threshold}$ epochs, the model is regarded as converged. Specifically, in our method, when we reach the epoch e^{min} , we incorporate two different factors to decrease the historical highest accuracy and increase the historical largest loss. This is because in our experiments, the model often achieves an artificially high accuracy and low loss at the beginning of training, which is not a desirable outcome. Therefore, by utilizing these factors, we aim to increase the likelihood of the neural network preserving the best parameters after reaching e^{min} .

Algorithm 1 Training Method

Require:

$[X^{train}, Y^{train}]$: Training Set
 $[X^{support}, Y^{support}]$: Support Set
 $[X^{help}, Y^{help}]$: Help Set
 θ : Network Parameter
 K : Kernal List of MK-MMD
 e^{min} : Minimum Training Epoch
 e^{max} : Maximum Training Epoch
 $e^{threshold}, \alpha \geq 1, \beta \leq 1$: Hyper-parameters for Early Stop

```

1: Initialize network Resnet and MLP
2: Set best history loss  $loss^{best} := \infty$ 
3: Set best history accuracy  $acc^{best} := 0$ 
4: Set epoch counters  $e^{acc} := 1, e^{loss} := 1$ 
5: for  $i = 1$  to  $e^{max}$  do
6:   Calculate embedding result  $E := \text{Resnet}(X)$ 
7:   Calculate classification result  $\hat{Y} = \text{MLP}(E)$ 
8:   Calculate loss function  $l^{train}$  according to Eq. 10
9:   Update network parameter  $\theta := \theta - \frac{dl^{train}}{d\theta}$ 
10:  Calculate cross entropy loss  $l$  in help set
11:  Calculate classification accuracy  $a$  in help set
12:  if  $a \geq acc^{best}$  then
13:    Update best history acc  $acc^{best} := a$ 
14:    Reset counter  $e^{acc} := 1$ 
15:    Save current parameter  $\theta$ 
16:  else
17:    Increment counter  $e^{acc} := e^{acc} + 1$ 
18:  end if
19:  if  $l \leq loss^{best}$  then
20:    Update best history loss  $loss^{best} := l$ 
21:    Reset counter  $e^{loss} := 1$ 
22:    Save current parameter  $\theta$ 
23:  else
24:    Increment counter  $e^{loss} := e^{loss} + 1$ 
25:  end if
26:  if  $i == e^{min}$  then
27:    Increase best history loss  $loss^{best} := loss^{best} \cdot \alpha$ 
28:    Decrease best history acc  $acc^{best} := acc^{best} \cdot \beta$ 
29:    Reset counters  $e^{acc} := 1, e^{loss} := 1$ 
30:  end if
31:  if  $i > e^{min}$   $\&\&$   $e^{loss} > e^{threshold}$   $\&\&$   $e^{acc} > e^{threshold}$  then ▷ Early Stop
32:    Break
33:  end if
34: end for

```

IV. EXPERIMENT

A. Dataset Description

In our experiment, we utilize two datasets: the publicly available WiGesture dataset [3] and a novel dataset named WiFall, which is proposed along with this paper. Both datasets are collected using the ESP32-S3 device and share the same data format, with a sample rate of 100Hz, 1 antenna, and 52 subcarriers. For our experiment, we divide the data into 1-second samples, resulting in each sample having a length of 100 data points.

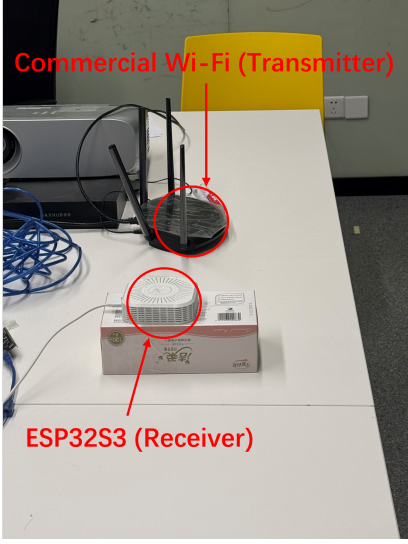


Fig. 6. Hardware: Our system utilizes a commercial Wi-Fi router as the transmitter (TX) and an ESP32-S3 as the receiver (RX). The ESP32-S3 decodes the received Channel State Information (CSI) and transmits it to a PC for inference.

After training, the model can be integrated into a real-time system, as shown in Fig. 6. In this system, a commercial Wi-Fi router continuously sends ping reply packets to the ESP32-S3. The ESP32-S3 extracts the CSI and forwards it to a PC equipped with an NVIDIA RTX 3090 GPU. The PC can then perform real-time inference using the trained neural network.

1) *WiGesture Dataset*: The WiGesture Dataset is a gesture recognition and people identification dataset. We use the dynamic part of the dataset that include 6 action id and 8 people id. The dataset is collected by 8 college students in a meeting room. The ESP32-S3 serves as receiver and a home Wi-Fi router serves as transmitter. The six actions include left-right, forward-backward, and up-down motions, clockwise circling, clapping, and waving. In the gesture recognition task, we consider different people as distinct domains. Similarly, in the people identification task, we treat different actions as separate domains.

2) *WiFall Dataset*: The data collection scenario and device are the same as the WiGesture dataset, as shown in Fig. 7. In the dataset, we have a total of 10 volunteers with an average age of 23.17, height of 1.75m, and BMI of 23.76. The activities include walking, jumping, sitting, standing up, and falling, which also consists of many types like forward fall, left fall, right fall, seated fall, and backward fall, shown as Fig. 8. Similar to the WiGesture Dataset, we consider different people as distinct domains. In our experiment, we use WiFall dataset to conduct action recognition tasks, where we identify five different actions, as well as fall detection tasks, where we only distinguish between fall and other actions.

B. Experiment Setup

Before conducting the experiment, we define the training set, support set, and testing set for each task in the n-shot scenarios as shown in Table III.

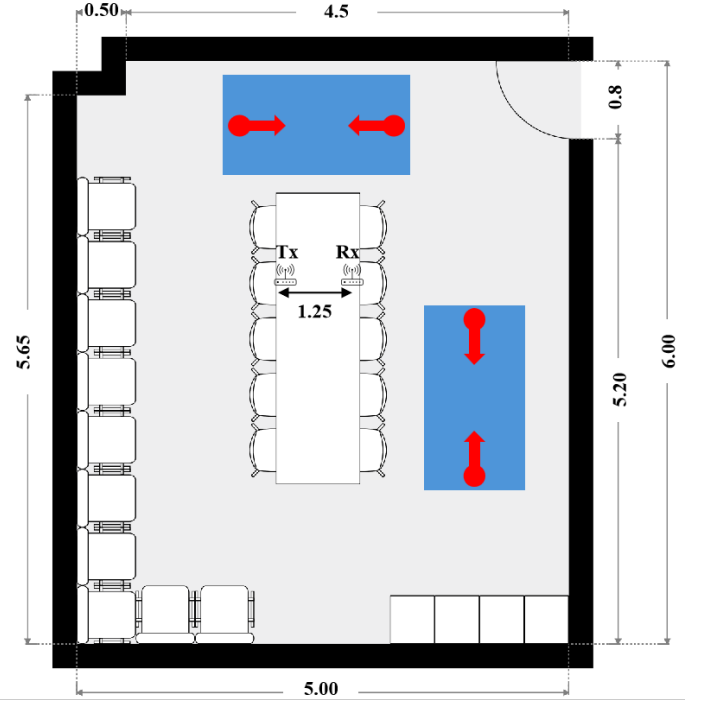


Fig. 7. Data Collection Environment of WiFall Dataset: The unit in the picture is meters.

The implementation details of our model are presented in Table IV. For our experiments, we utilized an Intel(R) Xeon(R) Silver 4210R CPU @ 2.40GHz and a NVIDIA RTX 3090 GPU as the hardware devices. During training, we observed that our model consumed approximately 2,500 MB of GPU memory.

C. Experiment Result

First, we present the experimental results in the one-shot and zero-shot scenarios as shown in Table V. Although Resnet18 [20] is not specifically designed for cross-domain scenarios, it is commonly used as a feature extractor in many related methods. Therefore, we include the results of Resnet in the in-domain scenario and zero-shot scenario as benchmarks. It can be seen that our KNN-MMD method shows excellent performance in each task, particularly outperforming all other methods in gesture recognition and action recognition tasks.

Then, as shown in Fig. 9, we illustrate the impact of the number of shots on classification accuracy. To assess the stability of our model, we also present shaded curves for our method and KNN by conducting five experiments. As mentioned earlier, it is challenging for other FSL methods to determine when the model is converged. Therefore, we directly use the best testing accuracy achieved by a particular FSL method during training as its accuracy. Even with this potentially unfair comparison mechanism, our KNN-MMD approach outperforms most conventional methods in all scenarios, which proves the efficiency of our local distribution approach. What's more, from the figure, it can be also observed that our model exhibits smaller fluctuations compared to vanilla KNN. This can be attributed to our preliminary

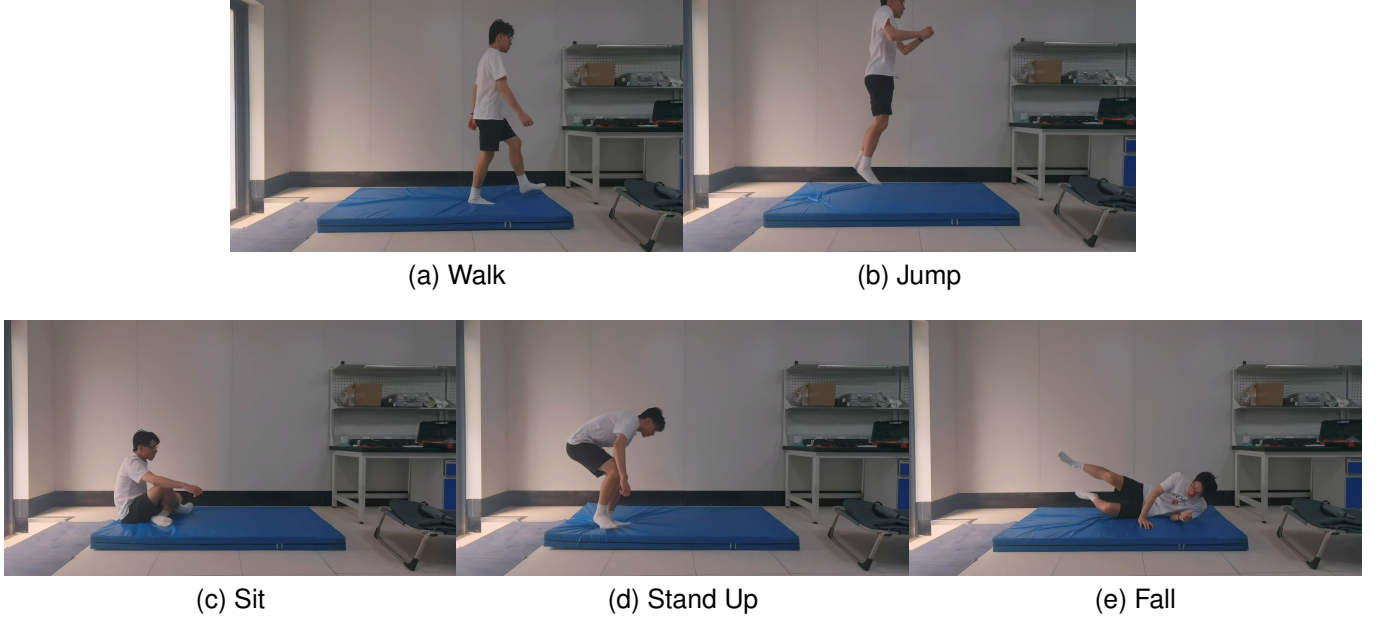


Fig. 8. Actions of WiFall Dataset

TABLE III
N-SHOT SCENARIO DESCRIPTION

Task	Training Set	Support Set	Testing Set
Gesture Recognition	People ID 1-7	n samples for each gesture in People ID 0	samples excluding support set in People ID 0
People Identification	Action ID 1-5	n samples for each person in Action ID 0	samples excluding support set in Action ID 0
Fall Detection & Action Recognition	People ID 1-9	n samples for each action in People ID 0	samples excluding support set in People ID 0

TABLE IV

MODEL CONFIGURATIONS: THIS TABLE PROVIDES A DETAILED OVERVIEW OF OUR KNN-MMD IN THE FOLLOWING EXPERIMENTS.

Configuration	Our Setting
CSI Sample Length	100
CSI Subcarrier Number	52
Batch Size	256
Input Dimension	(256,1,100,52)
Hidden Dimension of UMAP [19]	128
Hidden Dimension of Resnet [20]	64
Neighbor Number in KNN [21] : k	1
Selected Proportion in Support Set : $p\%$	50%
Optimizer	Adam
Learning Rate	0.0005
Hyper-parameters in Early Stop (Algorithm 1) [e^{\min} , e^{\max} , $e^{\text{threshold}}$, α , β]	[200,350,30,1.2,0.8]
Total Number of Parameters	11.21 million

classification mechanism. By using the confidence level to select the help set, our method's performance is less sensitive to the quality of the support set.

D. Comparison with Traditional DA Methods

In this section, we use the gesture recognition task to illustrate the shortcomings of traditional DA methods. For each type of method, we choose a specific model and compare it with our KNN-MMD.

1) *Metric-based Method*: For metric-based methods like KNN [21], the biggest problem is that they are heavily

influenced by the quality of the support set. As shown in Table VI, we reduced the data dimension in the target domain to d using UMAP and tested the KNN performance in an n -shot scenario with k nearest neighbors. Each scenario was tested 3 times, and the table shows the accuracy range. It can be seen that the accuracy fluctuates greatly, which may pose challenges for the practical application of this method. In Fig. 9, it can be seen that our KNN-MMD method does not exhibit such large fluctuations. Moreover, in Table VI, it's noticeable that our KNN-MMD is not very sensitive to the hyperparameters.

2) *Learning-based Method*: For learning-based methods, the biggest problem is that we do not know when to stop the training process. Fig. 10a illustrates the training process of a Siamese network [23], a traditional one-shot learning model. It can be seen that the performance change is relatively stable on the training set, but not on the testing set. However, during training, we do not have direct access to the performance on the testing set. This makes it very possible to stop the model training at an epoch that has worse performance on the testing set. Our KNN-MMD method efficiently solves this problem by using early stop according to the accuracy in the support set. In traditional learning-based methods, the support set also participates in training, so our early stop method cannot be used in them. Furthermore, as shown in Fig. 10c, the testing accuracy of our KNN-MMD also increases stably with the help of our local alignment mechanism.

3) *DAL Method*: As mentioned before, the global alignment operation of traditional DAL methods cannot guarantee

TABLE V
EXPERIMENTAL RESULTS: COMPARING THE BEST PERFORMANCE OF EACH METHOD. THE BOLD VALUE REPRESENTS THE CONSISTENTLY SUPERIOR RESULT WITHIN EACH SCENARIO, MAINTAINED ACROSS SUBSEQUENT TABLES.

Method	Scenario	Gesture Recognition	People Identification	Fall Detection	Action Recognition	Average Accuracy
Resnet18 [20]	in-domain	80.75%	86.75%	91.88%	70.50%	82.47%
	zero-shot	40.84%	70.50%	59.86%	26.00%	49.30%
Siamese [23]	one-shot	70.40%	82.87%	60.62%	38.95%	63.21%
AutoFi (MLP-based) [43]	one-shot	24.62%	24.71%	50.88%	23.59%	30.95%
AutoFi (CNN-based) [43]	one-shot	27.05%	36.14%	48.05%	26.95%	34.55%
Yang et al. [16]	one-shot	67.21%	74.22%	59.75%	48.52%	62.43%
Ding et al. [44]	one-shot	39.14%	70.94%	61.56%	30.37%	50.50%
CrossFi [18]	one-shot	91.72%	93.01%	80.93%	49.62%	78.82%
KNN [21]	one-shot	83.02%	82.67%	49.63%	46.87%	65.55%
KNN-MMD (Ours)	one-shot	93.26%	81.84%	77.62%	75.30%	82.01%
Ablation Study	one-shot	69.87%	73.78%	84.03%	74.06%	75.44%
MMD [25]	zero-shot	47.92%	67.25%	74.32%	45.61%	58.75%
MK-MMD [39]	zero-shot	40.36%	66.47%	72.26%	43.72%	55.70%
DANN [28]	zero-shot	41.41%	67.18%	74.06%	35.99%	54.66%
ADDA [45]	zero-shot	42.71%	65.43%	62.81%	36.08%	51.76%
GFK-KNN [26]	zero-shot	30.79%	51.50%	53.72%	34.17%	42.55%
CrossFi [18]	zero-shot	64.81%	72.79%	74.38%	40.46%	63.11%
Tian et al. [36]	zero-shot	68.13%	55.86%	61.72%	42.10%	56.95%
EEG [37]	zero-shot	59.75%	64.63%	69.53%	42.15%	59.02%

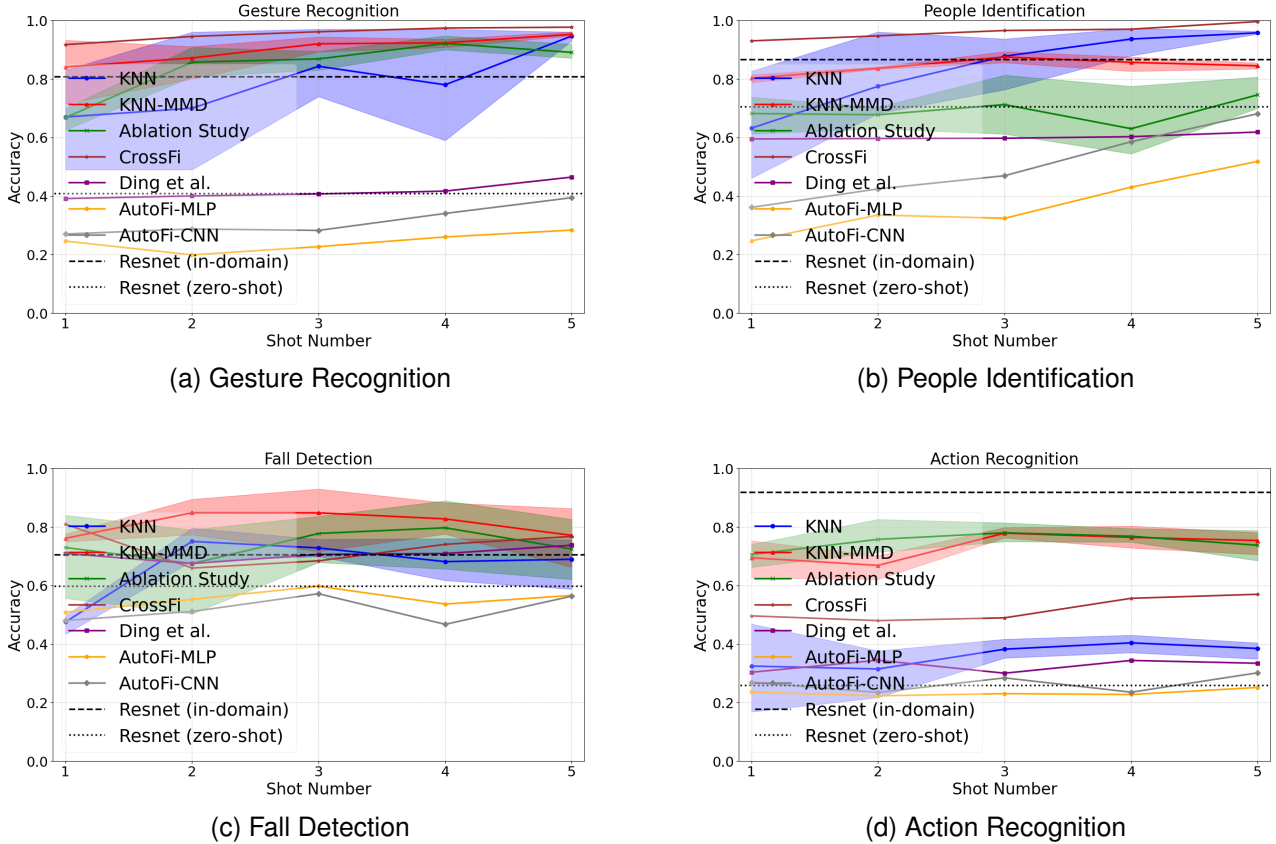


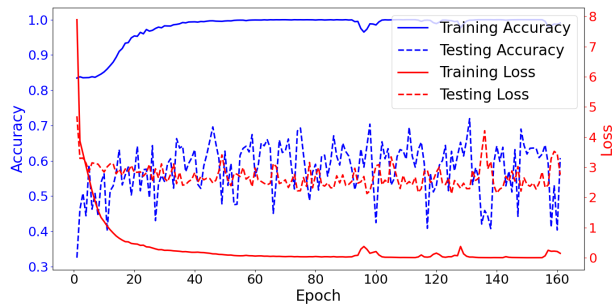
Fig. 9. Few-shot Experiment: The figures illustrate the influence of the number of shots on testing accuracy. The shaded area represents the range of accuracy observed across multiple experiments.

the model performance. In Fig. 11, we illustrate the UMAP result of different methods. It can be seen that the performance of the global alignment method MK-MMD does not differ much from ResNet, which even has no alignment operation. Even though they can split samples in the source domain (training set) well, achieving an accuracy over 99%, they

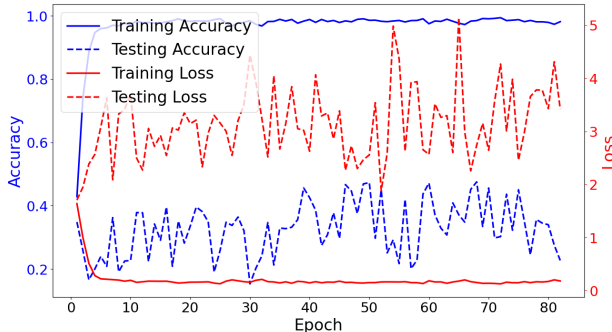
cluster samples in the target domain (testing set) chaotically. In contrast, our KNN-MMD still performs well in the target domain. As shown in Fig. 11c, it successfully aligns samples from the source domain and target domain within each category. Furthermore, in Fig. 11d, we show the upper bound performance of KNN-MMD, where we provide the ground

TABLE VI
PERFORMANCE OF KNN [21] AND OUR KNN-MMD: n DENOTES THE NUMBER OF SHOTS, k DENOTES THE NUMBER OF NEIGHBORS IN KNN, AND d DENOTES THE DATA DIMENSION AFTER REDUCTION USING UMAP [19].

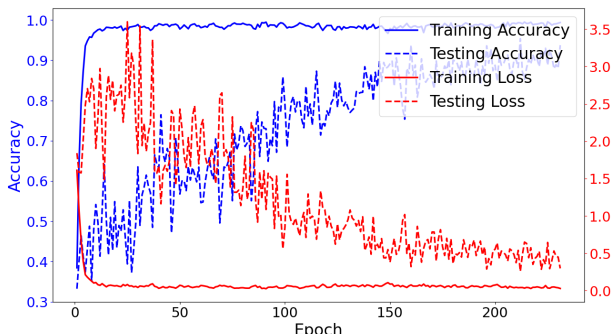
	KNN [21]			KNN-MMD		
	d=32	d=64	d=128	d=32	d=64	d=128
n=1, k=1	49%-83%	49%-69%	51%-83%	85%-95%	83%-93%	72%-93%
n=2, k=1	72%-92%	79%-89%	65%-96%	79%-94%	87%-93%	80%-91%
n=2, k=2	65%-76%	58%-82%	49%-83%	88%-95%	84%-92%	88%-91%
n=3, k=1	78%-94%	74%-93%	91%-97%	88%-95%	87%-95%	89%-92%
n=3, k=2	74%-94%	68%-97%	77%-82%	87%-93%	87%-91%	84%-92%
n=3, k=3	64%-93%	68%-94%	74%-91%	91%-96%	86%-90%	90%-94%
n=4, k=1	83%-97%	77%-97%	78%-97%	92%-96%	88%-92%	90%-93%
n=4, k=2	91%-96%	92%-97%	80%-95%	94%-98%	91%-94%	91%-96%
n=4, k=3	77%-97%	73%-97%	82%-92%	85%-93%	89%-93%	90%-94%
n=4, k=4	80%-95%	59%-88%	59%-97%	87%-94%	90%-94%	88%-95%



(a) Siamese Network [23]



(b) MK-MMD [39]



(c) KNN-MMD (shot number=1)

Fig. 10. Training Process of Different Methods

truth label of the help set instead of pseudo-labels. We notice that the cluster performance and accuracy of KNN-MMD and the upper bound do not have a significant difference, which proves the efficiency of our help set construction method. Finally, even though our early stop method can be used in most DAL methods, as the support set does not directly participate in training, limited by the model principle, even if we make it stop at the point with the best testing accuracy, it still has a poor performance, as shown in Fig. 6.

E. Ablation Study

In our KNN-MMD method, the MK-MMD seems unnecessary because we can simply pre-train the model on the training set and fine-tune it on the help set as many DA methods do. However, when choosing the top $p\%$ samples in the target domain, we cannot guarantee that the amounts of different category samples will be balanced. This imbalance may cause the long-tail problem during fine-tuning and significantly impact the network's performance. However, MMD is not affected by this issue. Furthermore, in extreme situations, some categories may be missing in the help set, which can be catastrophic for training the network. On the other hand, our method, which combines local MMD and global MMD, can mitigate this problem to some extent. We compare the performance of our method with that of fine-tuning a Resnet18 using help set in each task. As shown in Fig. 9, our MMD-based method shows better performance than the fine-tuning-based method. And in most tasks, our method also demonstrates better stability.

V. CONCLUSION

In this paper, we introduce KNN-MMD, a FSL method for cross-domain Wi-Fi sensing. We demonstrate that traditional DAL has its shortcomings and propose a local distribution alignment method to address this problem. Additionally, our method supports an early stop strategy to identify when to stop training, which is hardly used in most traditional FSL methods. The experimental results show that our model performs well and remains stable across various cross-domain WiFi sensing tasks, including gesture recognition, people identification, fall detection, and action recognition. The stability of our model also indicates its potential for practical applications.

In the future, there are several aspects of our method that can be further explored. Firstly, our method is not limited to

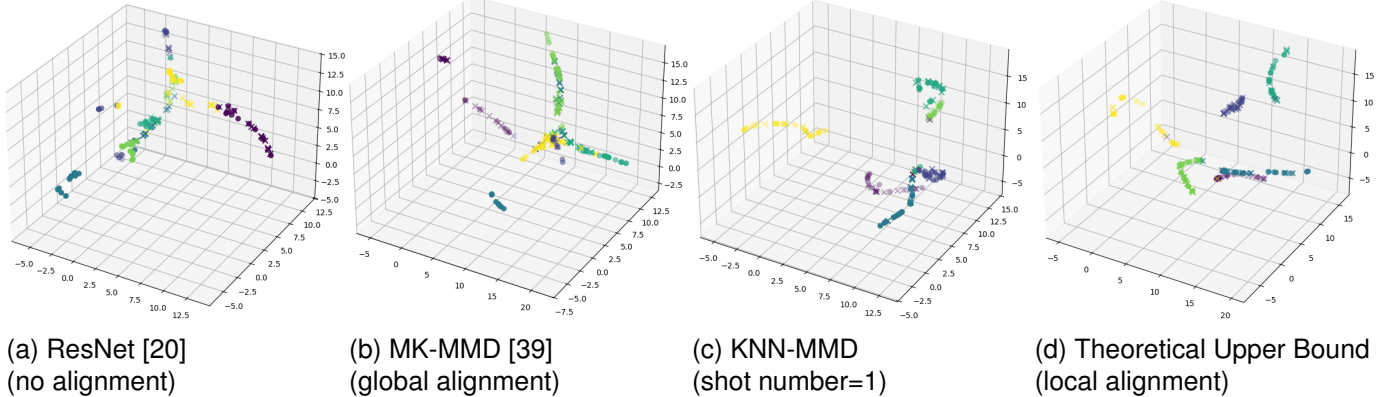


Fig. 11. Data Dimension Reduction Results of Embedding Results from Different Models: Different colors represent different categories. The circles represent samples from the source domain, and the crosses represent samples from the target domain.

KNN and MMD, and it would be interesting to investigate the effectiveness of other combinations of metric-based methods or few-shot learning methods with DAL methods. Additionally, by combining a zero-shot learning method with the DAL framework, we could also expand its range of applications. Moreover, the current framework could be used only for classification tasks. It would be worth exploring its application in regression tasks.

REFERENCES

- [1] T. Chen, X. Li, H. Li, and G. Zhu, “Deep learning-based fall detection using commodity wi-fi,” *Journal of Information and Intelligence*, 2024.
- [2] Z. Zhao, T. Chen, F. Meng, Z. Cai, H. Li, X. Li, and G. Zhu, “Lofi: Vision-aided label generator for wi-fi localization and tracking,” *arXiv preprint arXiv:2412.05074*, 2024.
- [3] Z. Zhao, T. Chen, F. Meng, H. Li, X. Li, and G. Zhu, “Finding the Missing Data: A BERT-inspired Approach Against Package Loss in Wireless Sensing,” *arXiv preprint arXiv:2403.12400*, 2024.
- [4] “Wi-fi® is an essential iot enabler,” 2023.
- [5] D. Halperin, W. Hu, A. Sheth, and D. Wetherall, “Tool release: Gathering 802.11 n traces with channel state information,” *ACM SIGCOMM computer communication review*, vol. 41, no. 1, pp. 53–53, 2011.
- [6] T. Ropault, S. Blandino, A. Sahoo, and N. T. Golmie, “Ieee 802.11bf: Enabling the widespread adoption of wi-fi sensing,” 2023-05-31 04:05:00 2023.
- [7] G. Zhu, D. Liu, Y. Du, C. You, J. Zhang, and K. Huang, “Toward an intelligent edge: Wireless communication meets machine learning,” *IEEE communications magazine*, vol. 58, no. 1, pp. 19–25, 2020.
- [8] G. Zhu, Z. Lyu, X. Jiao, P. Liu, M. Chen, J. Xu, S. Cui, and P. Zhang, “Pushing ai to wireless network edge: An overview on integrated sensing, communication, and computation towards 6g,” *Science China Information Sciences*, vol. 66, no. 3, p. 130301, 2023.
- [9] I. Nirmal, A. Khamis, M. Hassan, W. Hu, and X. Zhu, “Deep learning for radio-based human sensing: Recent advances and future directions,” *IEEE Communications Surveys & Tutorials*, vol. 23, no. 2, pp. 995–1019, 2021.
- [10] H. Chen, H. Chen, Z. Zhao, K. Han, G. Zhu, Y. Zhao, Y. Du, W. Xu, and Q. Shi, “An overview of domain-specific foundation model: key technologies, applications and challenges,” *arXiv preprint arXiv:2409.04267*, 2024.
- [11] Z. Han, L. Guo, Z. Lu, X. Wen, and W. Zheng, “Deep adaptation networks based gesture recognition using commodity wifi,” in *2020 IEEE Wireless Communications and Networking Conference (WCNC)*, pp. 1–7, IEEE, 2020.
- [12] X. Ding, T. Jiang, Y. Li, W. Xue, and Y. Zhong, “Device-free location-independent human activity recognition using transfer learning based on cnn,” in *2020 IEEE International Conference on Communications Workshops (ICC Workshops)*, pp. 1–6, IEEE, 2020.
- [13] M. Zhou, Y. Li, L. Xie, and W. Nie, “Maximum mean discrepancy minimization based transfer learning for indoor wlan personnel intrusion detection,” *IEEE Sensors Letters*, vol. 3, no. 8, pp. 1–4, 2019.
- [14] Z. Gao, Y. Gao, S. Wang, D. Li, and Y. Xu, “Crisloc: Reconstructable csi fingerprinting for indoor smartphone localization,” *IEEE Internet of Things Journal*, vol. 8, no. 5, pp. 3422–3437, 2020.
- [15] H. He, X. Huan, J. Wang, Y. Luo, H. Hu, and J. An, “P 3 id: A privacy-preserving person identification framework towards multi-environments based on transfer learning,” *IEEE Transactions on Mobile Computing*, 2024.
- [16] J. Yang, H. Zou, Y. Zhou, and L. Xie, “Learning gestures from WiFi: A Siamese recurrent convolutional architecture,” *IEEE Internet of Things Journal*, vol. 6, no. 6, pp. 10763–10772, 2019.
- [17] D. Wang, J. Yang, W. Cui, L. Xie, and S. Sun, “Airfi: empowering wifi-based passive human gesture recognition to unseen environment via domain generalization,” *IEEE Transactions on Mobile Computing*, 2022.
- [18] Z. Zhao, T. Chen, Z. Cai, X. Li, H. Li, Q. Chen, and G. Zhu, “Crossfi: A cross domain wi-fi sensing framework based on siamese network,” *arXiv preprint arXiv:2408.10919*, 2024.
- [19] L. McInnes, J. Healy, and J. Melville, “Umap: Uniform manifold approximation and projection for dimension reduction,” *arXiv preprint arXiv:1802.03426*, 2018.
- [20] K. He, X. Zhang, S. Ren, and J. Sun, “Deep residual learning for image recognition,” in *Proceedings of the IEEE conference on computer vision and pattern recognition*, pp. 770–778, 2016.
- [21] L. E. Peterson, “K-nearest neighbor,” *Scholarpedia*, vol. 4, no. 2, p. 1883, 2009.
- [22] M. Ahmed, R. Seraj, and S. M. S. Islam, “The k-means algorithm: A comprehensive survey and performance evaluation,” *Electronics*, vol. 9, no. 8, p. 1295, 2020.
- [23] J. Bromley, I. Guyon, Y. LeCun, E. Säckinger, and R. Shah, “Signature verification using a ‘siamese’ time delay neural network,” *Advances in neural information processing systems*, vol. 6, 1993.
- [24] E. Hoffer and N. Ailon, “Deep metric learning using triplet network,” in *Similarity-Based Pattern Recognition: Third International Workshop, SIMBAD 2015, Copenhagen, Denmark, October 12–14, 2015. Proceedings 3*, pp. 84–92, Springer, 2015.
- [25] A. Gretton, K. M. Borgwardt, M. J. Rasch, B. Schölkopf, and A. Smola, “A kernel two-sample test,” *The Journal of Machine Learning Research*, vol. 13, no. 1, pp. 723–773, 2012.
- [26] B. Gong, Y. Shi, F. Sha, and K. Grauman, “Geodesic flow kernel for unsupervised domain adaptation,” in *2012 IEEE conference on computer vision and pattern recognition*, pp. 2066–2073, IEEE, 2012.
- [27] J. Zhang, G. Zhu, R. W. Heath Jr, and K. Huang, “Grassmannian learning: Embedding geometry awareness in shallow and deep learning,” *arXiv preprint arXiv:1808.02229*, 2018.
- [28] Y. Ganin, E. Ustinova, H. Ajakan, P. Germain, H. Larochelle, F. Laviolette, M. March, and V. Lempitsky, “Domain-adversarial training of neural networks,” *Journal of machine learning research*, vol. 17, no. 59, pp. 1–35, 2016.
- [29] P. Zhu, X. Zhang, X. Han, X. Cheng, J. Gu, P. Chen, and L. Jiao, “Cross-domain classification based on frequency component adaptation

- for remote sensing images,” *Remote Sensing*, vol. 16, no. 12, p. 2134, 2024.
- [30] B. He, Y. Chen, D. Zhu, and Z. Xu, “Domain adaptation via wasserstein distance and discrepancy metric for chest x-ray image classification,” *Scientific Reports*, vol. 14, no. 1, p. 2690, 2024.
 - [31] L. Torrey and J. Shavlik, “Transfer learning,” in *Handbook of research on machine learning applications and trends: algorithms, methods, and techniques*, pp. 242–264, IGI global, 2010.
 - [32] T. Hospedales, A. Antoniou, P. Micaelli, and A. Storkey, “Meta-learning in neural networks: A survey,” *IEEE transactions on pattern analysis and machine intelligence*, vol. 44, no. 9, pp. 5149–5169, 2021.
 - [33] Y. Wang, Q. Yao, J. T. Kwok, and L. M. Ni, “Generalizing from a few examples: A survey on few-shot learning,” *ACM computing surveys (csur)*, vol. 53, no. 3, pp. 1–34, 2020.
 - [34] J. Huang, A. Gretton, K. Borgwardt, B. Schölkopf, and A. Smola, “Correcting sample selection bias by unlabeled data,” *Advances in neural information processing systems*, vol. 19, 2006.
 - [35] R. Gopalan, R. Li, and R. Chellappa, “Domain adaptation for object recognition: An unsupervised approach,” in *2011 international conference on computer vision*, pp. 999–1006, IEEE, 2011.
 - [36] Y. Tian and B. Li, “K-Nearest Neighbor based local distribution alignment,” in *International Conference on Intelligent Computing*, pp. 470–480, Springer, 2022.
 - [37] Z. Li, E. Zhu, M. Jin, C. Fan, H. He, T. Cai, and J. Li, “Dynamic domain adaptation for class-aware cross-subject and cross-session EEG emotion recognition,” *IEEE Journal of Biomedical and Health Informatics*, vol. 26, no. 12, pp. 5964–5973, 2022.
 - [38] G. Csurka, “Domain adaptation for visual applications: A comprehensive survey,” *arXiv preprint arXiv:1702.05374*, 2017.
 - [39] A. Gretton, D. Sejdinovic, H. Strathmann, S. Balakrishnan, M. Pontil, K. Fukumizu, and B. K. Sriperumbudur, “Optimal kernel choice for large-scale two-sample tests,” *Advances in neural information processing systems*, vol. 25, 2012.
 - [40] Z. Cai, T. Chen, F. Zhou, Y. Cui, H. Li, X. Li, G. Zhu, and Q. Shi, “Falldevideo: Vision-aided wireless sensing dataset for fall detection with commodity wi-fi devices,” in *Proceedings of the 3rd ACM MobiCom Workshop on Integrated Sensing and Communications Systems*, pp. 7–12, 2023.
 - [41] G. Zhu, B. Wang, W. Gao, Y. Hu, C. Wu, and K. R. Liu, “Srcsense: Robust wifi-based motion source recognition via signal-informed deep learning,” *IEEE Journal of Selected Areas in Sensors*, 2024.
 - [42] M. Sugiyama, M. Krauledat, and K.-R. Müller, “Covariate shift adaptation by importance weighted cross validation..,” *Journal of Machine Learning Research*, vol. 8, no. 5, 2007.
 - [43] J. Yang, X. Chen, H. Zou, D. Wang, and L. Xie, “AutoFi: Toward Automatic Wi-Fi Human Sensing via Geometric Self-Supervised Learning,” *IEEE Internet of Things Journal*, vol. 10, no. 8, pp. 7416–7425, 2022.
 - [44] X. Ding, T. Jiang, Y. Zhong, S. Wu, J. Yang, and W. Xue, “Improving WiFi-based human activity recognition with adaptive initial state via one-shot learning,” in *2021 IEEE Wireless Communications and Networking Conference (WCNC)*, pp. 1–6, IEEE, 2021.
 - [45] E. Tzeng, J. Hoffman, K. Saenko, and T. Darrell, “Adversarial discriminative domain adaptation,” in *Proceedings of the IEEE conference on computer vision and pattern recognition*, pp. 7167–7176, 2017.